Research Paper

Advances in Structural Engineering

Advances in Structural Engineering
2024, Vol. 27(13) 2338–2358

DOI: 10.1177/13694332241268186
journals.sagepub.com/home/ase
Sage

Flexural performance of the negative moment region in bonded steel-wire-rope-strengthened reinforced concrete T-beams at different prestressing levels

Yanuar Haryanto[1,2], Gathot Heri Sudibyo[1], Laurencius Nugroho[3], Hsuan-Teh Hu[3,4], Ay Lie Han[5], Fu-Pei Hsiao[6], Arnie Widyaningrum[1] and Yudi Susetyo[1]

Abstract

This work examines the performance of reinforced concrete (RC) beams strengthened using bonded steel wire rope (SWR) at various prestressing levels. The strengthening approach has, however, been applied to the flexural strengthening of RC T-beams in the negative moment region, in order to determine its advantages. For this purpose, four RC T-beams were fabricated and tested under monotonic four-point bending: one control beam (S00), one beam strengthened with non-prestressed SWR (S20), and two beams strengthened with SWR (prestressed at 10% and 20% of their ultimate tensile strength: S21 and S22). The results indicate that the strengthened beams exhibit higher load-carrying capacities. Specifically, the cracking load, yield load, and ultimate load of S20, S21, and S22 increase by 10%–30%, 30%–50%, and 50%–90%, respectively, compared to S00. Additionally, there is an improvement in stiffness and energy absorption capacity. However, these strategies may have a dual effect on the specimens, resulting in a reduction in their ductility index. Finally, the tested beams were replicated using a three-dimensional finite element model, which has proved effective in predicting the behavior of such structures and, therefore, was found to be appropriate for use in future studies.

Keywords

reinforced concrete T-beam, negative moment region, steel wire rope, strengthening, prestressing level, flexural performance

[1]Department of Civil Engineering, Faculty of Engineering, Jenderal Soedirman University, Purwokerto, Indonesia
[2]TRD Research Centre, Institute for Research and Community Service, Jenderal Soedirman University, Purwokerto, Indonesia
[3]Department of Civil Engineering, College of Engineering, National Cheng Kung University, Tainan, Taiwan
[4]Department of Civil and Disaster Prevention Engineering, College of Engineering and Science, National United University, Miaoli, Taiwan
[5]Department of Civil Engineering, Faculty of Engineering, Diponegoro University, Semarang, Indonesia
[6]National Center for Research on Earthquake Engineering, National Applied Research Laboratories, Taipei, Taiwan

Corresponding authors:

Yanuar Haryanto, Department of Civil Engineering, Faculty of Engineering, Jenderal Soedirman University, Jl Mayjen Sungkono KM 5, Purwokerto 53122, Indonesia.
Email: yanuar.haryanto@unsoed.ac.id

Gathot Heri Sudibyo, Department of Civil Engineering, Faculty of Engineering, Jenderal Soedirman University, Jl Mayjen Sungkono KM 5, Purwokerto 53122, Indonesia.
Email: gathot.sudibyo@unsoed.ac.id

Laurencius Nugroho, Department of Civil Engineering, College of Engineering, National Cheng Kung University, No. 1 University Road, Tainan 70101, Taiwan.
Email: laurenciusnugroho@gmail.com

Hsuan-Teh Hu, Department of Civil Engineering, College of Engineering, National Cheng Kung University, No. 1 University Road, Tainan 70101, Taiwan.
Email: hthu@mail.ncku.edu.tw

Introduction

In recent years, it has become increasingly common to enhance the structural behavior of undamaged structures and restore the performance of damaged structures (because of inadequate maintenance, design flaws, or post-accident rehabilitation). This also enables the repurposing of older structures that fail to meet the more stringent serviceability requirements of current codes (Haryanto et al., 2021b). Hence, it seems prudent to rejuvenate older districts in urban areas, which should be regarded as a distinct objective in the foreseeable future. Reconstructing older buildings, as opposed to constructing new ones, offers the potential to minimize the environmental consequences associated with demolition and subsequent construction (Haryanto et al., 2021c; Mukhtar and Faysal, 2018). This makes it imperative to study current strategies to strengthen and repair existing structures and, at the same time, discover and learn new ones.

Non-metallic materials such as bamboo (Haryanto et al., 2017b; Hidayat et al., 2019; Nahar and Rahman, 2015; Sen and Reddy, 2011; Xu et al., 2019), poly-urethane-cement (Hussain et al., 2013), textile-reinforced mortar (Raoof et al., 2017), textile-reinforced geopolymer mortar (Zhang et al., 2019), textile-reinforced concrete (Yin et al., 2014), engineered cementitious composite (Hung et al., 2023), and ultrahigh-performance concrete (Hung et al., 2021), have been employed to restore or improve the performance of reinforced concrete (RC) structures. In the last few decades, fiber-reinforced polymer (FRP) materials have emerged as promising alternative repair materials due to several characteristics, such as a greater strength to weight ratio, greater corrosion resistance, convenient usage, negligible alteration of the member structure, and high resistance to insect and fungal growth (Han et al., 2022; Haryanto et al., 2021e, 2022; Siddika et al., 2020). Several studies have highlighted the improvements in the flexural capacity of slabs and beams through the application of externally-bonded FRP (Bencardino et al., 2006; Choobbor et al., 2019; Gudonis et al., 2014; Ism and Rabie, 2019; Lesmana et al., 2013; Lesmana and Hu, 2014, 2015; Razaqpur et al., 2020; Siddika et al., 2019; Teng et al., 2003; Tudjono et al., 2015). This material has also been found to improve a beam's shear capacity (Lee et al., 2017; Al-Rousan, 2017; Oller et al., 2019; Abuodeh et al., 2020; Zhou et al., 2020; Saribiyik et al., 2021), confinement effect and column flexibility or ductility (Amran et al., 2018), as well as the seismic performance of walls (Papanicolaou et al., 2008) and beam-column joints (Attari et al., 2019). However, FRP also has some disadvantages, such as lower resistance when subjected to high temperatures, a chance of sudden failure without prior warning, the impossibility of its application in certain humid or cold areas, and incompatibility with the concrete substrate (Firmo et al., 2015; Peled, 2007; Zhang et al., 2019). As a result, there are certain restrictions on its use and the majority of them are related to attaching fibers to organic resin, as in the case of epoxy.

The utilization of metallic materials as a strengthening technique has also gained popularity and been proven to be an effective method for strengthening RC structures. The behavior of RC structures strengthened with metallic materials has been the subject of numerous studies. The application of a steel plates strengthening system in RC structures represents one of the pioneering methods introduced in the last century for structural improvement utilizing metallic materials (Jones et al., 1988). Nevertheless, a significant issue that has been identified in steel plates is their inadequate corrosion resistance (Qestha et al., 2016). Exposure tests conducted by Raithby (1982) and MacDonald and Calder (1982) revealed that a significant amount of corrosion takes place at the interface between steel and epoxy. This corrosion leads to a reduction in strength and localized debonding.

Different kinds of metallic material that can be utilized to strengthen RC structures include steel bars, steel clamps, stainless steel, and aluminum plates. Hosen et al. (2014) conducted an experiment to study the flexural strengthening of RC beams using the near surface mounted (NSM) technique with varying ratios of steel bars. The results demonstrated an increase in flexural strength, as well as improvements in energy and deflection ductility. By using steel clamps, the ductility of the strengthened beams increased approximately tenfold and the failure behavior changed from brittle to ductile (Demir et al., 2018). Franco et al. (2018) tested RC T-beams strengthened with stainless steel and found that increasing the flexural stiffness of the beams was achievable with all strengthening approaches. In order to address the challenge of handling steel on site (due to its heavy weight), the fabrication of aluminum plates can serve as external strengthening materials (Abdalla et al., 2016; Abu-Obeidah, 2015; Fayed et al., 2019; Rasheed et al., 2017).

Due to its high strength, light weight, and high flexibility characteristics, steel wire rope (SWR), which is typically used in mechanical applications (Fontanari et al., 2015), is also a material that shows potential for strengthening RC structures. The performance of SWR-strengthened RC structures has been examined by several researchers (Kim et al., 2007; Li et al., 2018; Sim et al., 2009; Yang et al., 2009a, 2009b, 2012; Yang and Ashour, 2007). Additionally, Wu et al. (2010, 2014) conducted a study examining the flexural behavior of RC beams, strengthened using prestressed-SWR (P-SWR). The study involved both experimental and theoretical investigations. Wei and Wu (2014) also considered concrete columns strengthened by confining them with SWRs and studying their compression behavior; the outcomes and conclusions were provided in the JGJ/T325-2014 guide (Ministry of Housing and Urban-Rural Development of China, 2014). The performance of two SWRs with a diameter of 6 mm, used to externally strengthen RC beams with various end anchors, was examined by Haryanto et al. (2018). The findings demonstrated that end-anchor types 1 and 2 had ratios that tended towards one for every parameter, indicating that they both provided an equal and significant contribution to the performance of the steel wire rope. Moreover, Haryanto et al. (2021a) stated, in a continuation investigation with different numbers and diameters of external SWRs, that there was an increase in ultimate load by up to 2.5 times. Specimens with fewer SWRs showed better ductility and stiffness improvements compared to those with more SWRs (which experienced slippage at the end-anchors). However, overlooked applications, such as flexural strengthening in the negative moment region of RC T-beams, need further study; the P-SWRs strengthening system could be adapted for flexible use in these regions.

Research significance

This work addresses the critical challenges in strengthening the negative moment region of concrete members, which is more complex than the positive moment region and is often overlooked in favor of it, highlighting a distinctive aspect of this investigation. Jumaat et al. (2014) mentioned several practical issues in this context, emphasizing that the negative moment region of a continuous span is crucial due to the simultaneous presence of maximum bending moments and shear forces, as illustrated in Figure 1. Additionally, the presence of columns often obstructs the arrangement of a strengthening system over the web portion of the beam (Al-Khafaji and Salim, 2020). Previous studies have demonstrated that installing strengthening materials in the negative moment region of RC beams enhances their load-carrying capacity and flexural stiffness (Grace, 2001; Tudjono, 2018).

The current paper is a continuation study that broadens the scope of the previous research by Haryanto et al. (2017a, 2019, 2023). It aims to examine the technique

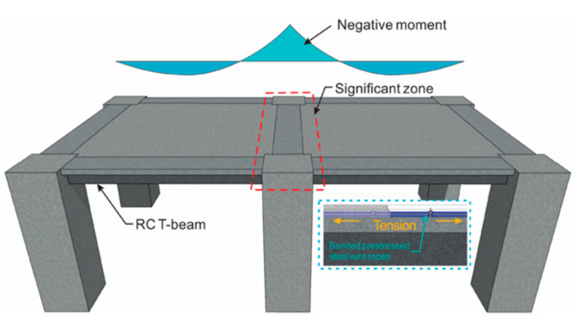

Figure 1. Negative moment region of a structure.

for strengthening RC beams with bonded P-SWRs positioned in the negative moment region. The process involved the implementation of various prestressing levels for SWRs and the casting of cement mortar as a bond to prevent SWRs from corrosion. Moreover, the strengthening effects of the bonded P-SWRs on the performance of the beams were studied by considering the appropriate variables. A four-point bending arrangement was also used to show the failure response of the four specimens. The outcomes were used to shed light on the flexural load-carrying capacity, deflection behavior, and failure modes, as well as to estimate the ductility index, stiffness, energy absorption capacity, strain response, and other properties of the beams. This was followed by the simulation of the flexural behavior of the beams strengthened using bonded P-SWRs in the negative moment region, using a 3D finite element (FE) model. The accuracy of this model was validated by comparing the results with the experimental data obtained from the specimens tested.

Experimental program

Geometric features

Figure 2 displays the general elevation view of the unstrengthened and strengthened beam specimens, as well as their cross-sectional details, respectively. The specimens were designed to fail in flexure as tension-controlled beams, according to code ACI 318-19 (American Concrete Institute, 2019). Normal concrete, made using ordinary Portland cement as the binder, along with locally sourced river sand and crushed stone with a maximum size of 20 mm as fine and coarse aggregates, was used to cast four RC T-beams. The total height was 250 mm, the web width was 150 mm, the flange width was 400 mm, the flange depth was 75 mm, and the span was 2400 mm. Moreover, three deformed steel rebars, each of 13 mm diameter, were used to reinforce the beams in the tensile zone, while two plain steel rebars of 8 mm diameter were applied to the beams' cross-section in the compression zone. The same beams were also reinforced by attaching 8 mm diameter stirrups, such that they were 100 mm distant from each other in the center span and 40 mm in the shear span.

One of the four beams was used as the control beam and was not subjected to any strengthening or prestressing. Another beam was subjected to strengthening through bonded SWRs but was not prestressed, while the last two beams were strengthened using SWRs that had been prestressed at 10% and 20% of their ultimate tensile strength. These prestressing levels are manageable in a real-world environment and can be realistically implemented in construction and strengthening projects. Moreover, a cementitious overlay that was relatively simple and inexpensive to enhance the load-carrying capacity and stiffness efficiently (Lampropoulos et al., 2016; Qasim et al., 2023; Shang et al., 2019; Yang et al., 2018), was used to bond the SWRs along the specimens lengthwise, incorporating 40 mm thick mortar. It is important to note that the second digit of the beam code denotes the number of SWRs used as strengthening material, while the third digit represents the prestressing level.

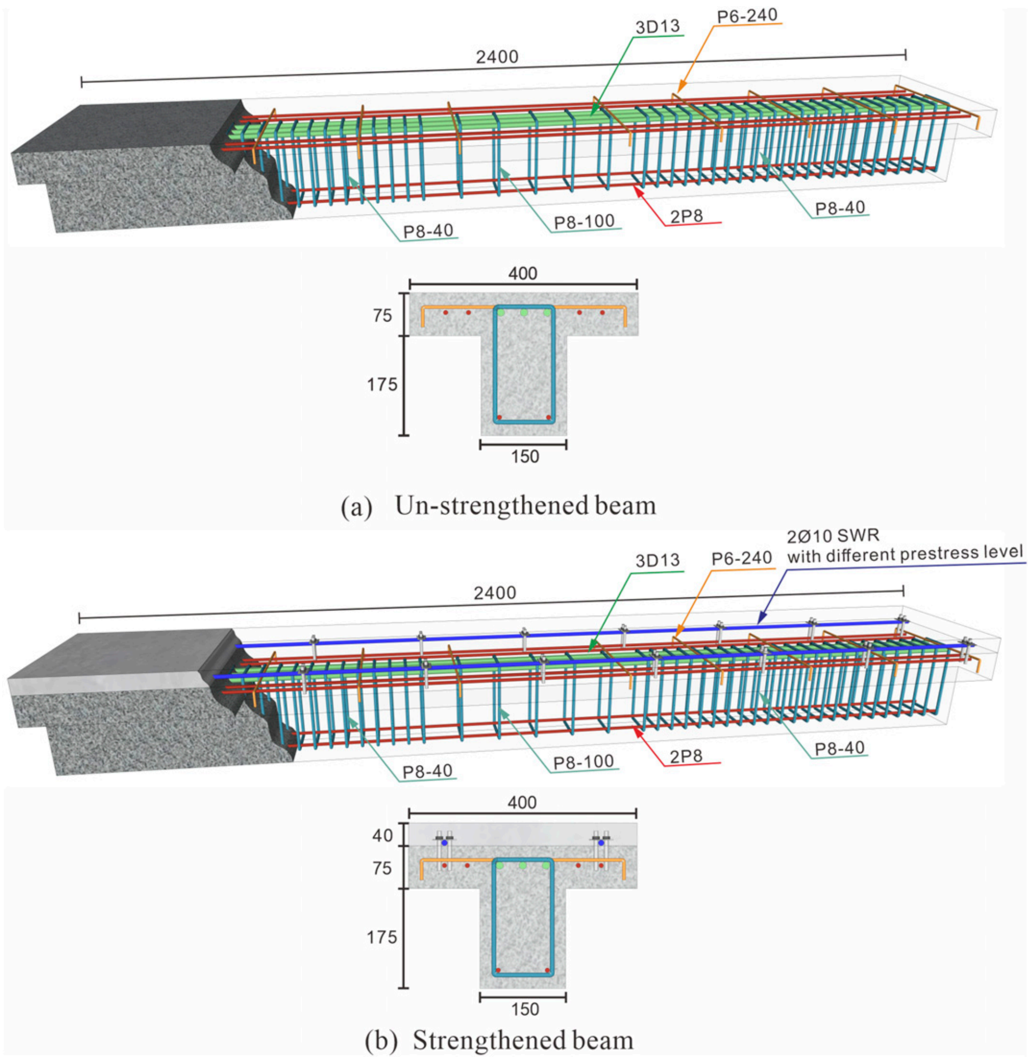

Figure 2. Geometric details of tested specimens (unit: mm).

Table 1. Description of tested specimens.

						Longitudinal reinforcement		Stirrup			
Specimens	L (mm)	bf (mm)	tf (mm)	bw (mm)	tw (mm)	Top	Bottom	Shear span	Center span	SWR	Prestressing level (%)
S00	2400	400	75	150	175	3D13	2P8	P8-40	P8-100	–	–
S20	2400	400	115	150	175	3D13	2P8	P8-40	P8-100	2ϕ10	0
S21	2400	400	115	150	175	3D13	2P8	P8-40	P8-100	2ϕ10	10
S22	2400	400	115	150	175	3D13	2P8	P8-40	P8-100	2ϕ10	20

Table 1 indicates the designations and detailed information on the RC T-beam specimens.

Material properties

The compressive strength of concrete was examined by conducting tests on six standard cylinder specimens measuring 150 × 300 mm. These tests were carried out following the guidelines outlined in ASTM C39/C39M-21 (ASTM International, 2021). The specimens were prepared using the same mixture that was used for casting the beams. An average concrete compressive strength of 32.39 MPa was achieved after 28 days of casting. Moreover, hot-rolled plain and deformed steel rebars, as well as stirrups, were employed to reinforce the specimen in line with SNI 2052: 2014 (National Standardization Agency of Indonesia, 2014). The mechanical properties of the steel rebars and SWRs were examined using uniaxial coupon tensile tests in accordance with the guidelines outlined in ASTM A370-18 (ASTM International, 2018). The plain (8 mm diameter) steel rebars were found to have an average elastic modulus of 201.64 GPa, a yield strength of 373.85 MPa, and an ultimate tensile strength of 525.33 MPa. The deformed 13 mm diameter steel rebars recorded values of 197.66 GPa, 479.71 MPa, and 742.52 MPa, respectively. The SWR normally has six helically arranged strands on the surface of the central core (Lee, 1991; Raoof and Davies, 2003), which is made up of a small independent wire rope core (IWRC), as shown in Figure 3. The 10 mm diameter SWRs were found to have an average elastic modulus equivalent to 132.57 GPa and an average ultimate tensile strength of 743.73 MPa. Meanwhile, steel plates and 8 mm diameter Dynabolts, with a 14.50 kN average shear strength, were used to fasten and anchor the SWRs, as depicted in Figure 4. The compressive strength of the mortar used to bond this configuration (see Figure 5) was evaluated using 50 mm cube specimens in accordance with the ASTM C109/C109M-20 standard (ASTM International, 2020). An average compressive strength of 49.85 MPa was achieved for the mortar after 28 days of casting.

Figure 3. Steel wire rope.

Prestressing procedure

The present study involved the application of a prestressing force to the SWR, using the pretensioned system that was designed and installed at the structural laboratory of Jenderal Soedirman University. This system was implemented following the methodology proposed by Tehrani et al. (2019), as illustrated in Figure 6. In summary, a hydraulic jack with a 1000 kN capacity was employed to apply tension to the SWR at one end, while an anchor was utilized to secure the SWR at the opposite end (referred to as the ‘dead end’). Strain gauges were used to control the prestress level during the prestressing process. Continuous monitoring of the strain gauge data was conducted throughout the entire duration required for the mortar to be

Figure 4. Steel plate and dynabolts.

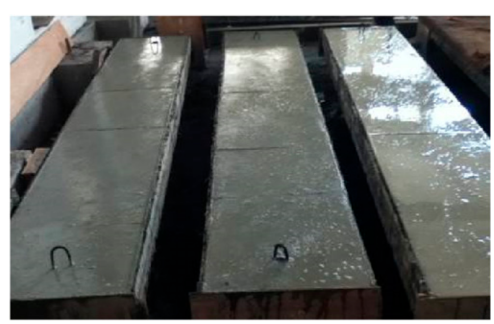

Figure 5. Cementitious adhesive.

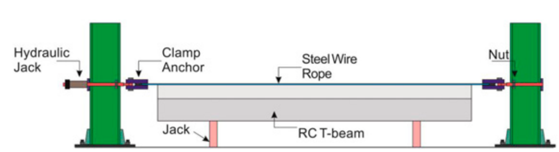

Figure 6. Schematic drawing of the prestressing equipment.

cured. This monitoring also covered the release of the prestressing force and the subsequent testing period. After applying the desired prestressing force, the SWR was secured at the jacking end. The prestressing force was released once the mortar had finished curing. Ultimately, the clamp anchors were taken out once the prestressing force in the SWR was successfully transferred to the beam. It is important to mention that two jacks were employed to stabilize the specimen while undergoing the prestressing procedure.

Loading configuration

To simulate the structural behavior of the RC T-beam specimen in the negative moment region, where the flange is subjected to a tensile strain and the web experiences a compressive strain, a reverse loading scheme was adopted in the experiment. The four-point bending test was conducted by applying a concentrated vertical symmetric load to the web of the beam, using a distribution beam constructed from steel sections, which ensured that the 50 cm area in the mid-span was a pure bending region. The test setup and the instrumentation are illustrated in Figure 7. From top to bottom, the loading system consisted of an electro-hydraulic servo press with a 1000 kN capacity, pressure sensor, spreader beam, test beam, and roller support. The force control was adopted until the test beams experienced failure. For this purpose, each step increased by 2 kN and, during the loading process, it was necessary to observe the formation of cracks in the specimen. The position and direction of the cracks were appropriately delineated by a pen. Simultaneously, the deflection data were recorded from the displacement sensor and the compressive strain of concrete was defined using a strain gauge.

The test involved measuring various parameters, including test load, vertical deflection, compressive strain of the concrete, and specimen crack formation. The measurement methods were, specifically: (1) the magnitude of the applied load was measured by a pressure sensor; (2) the vertical deflection was measured via the linear variable differential transformers (LVDTs). During the test, three LVDTs were placed in the left loading point section, the midspan section, and the right loading point section. These LVDTs were utilized to measure the deflection at each respective location; (3) the compressive strain of concrete was measured by a strain gauge with a gauge length of 30 mm attached to the midpoint of the upper surface of the specimen; and (4) the crack formation was observed using a crack observation instrument.

Experimental results and evaluation

The research involved experimental exploration of the performance demonstrated by prestressed-SWR-strengthened RC T-beams in the negative moment region. This was implemented through continuous observation of the loading behavior and relevant deflections, starting from the crack initiation point and up until the ultimate stage. Moreover, attention was also paid to the behavior at different prestressing levels and the summary of all values obtained from the experiment is presented in Table 2. The following sections discuss the outcomes of the experiment.

Loads

The control beam exhibits the lowest crack initiation load or cracking load, compared to that of the strengthened beams. With the implementation of the bonded SWRs, prior to prestressing, an approximately 11.19% increase in crack initiation load was observed, compared to that of the control specimen. The crack initiation load for the beams with prestressed bonded SWRs was further increased by 13.64% and 20.98% for S21 and S22, respectively, compared to that of the control specimen, as shown in Figure 8. The enhanced cracking loads are attributed to the

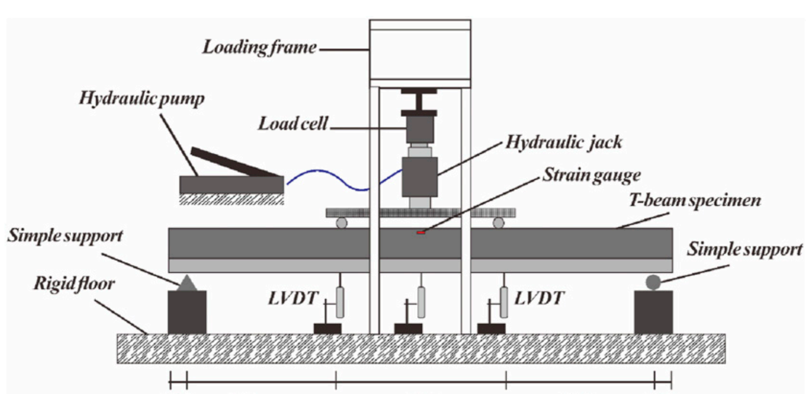

Figure 7. Experimental setup (units: mm).

Table 2. Summary of the test results.

	Load capacity (kN)			Deflection (mm)			
Specimens	Cracking	Yield	Ultimate	Cracking	Yield	Ultimate	Failure mode
S00	28.60	72.10	88.50	2.00	8.19	52.72	Flexural failure
S20	31.80	93.80	140.80	2.05	8.59	30.44	Flexural failure
S21	32.50	98.10	150.10	2.32	10.79	36.39	Flexural failure
S22	34.60	106.30	167.50	2.40	11.49	37.52	Flexural failure

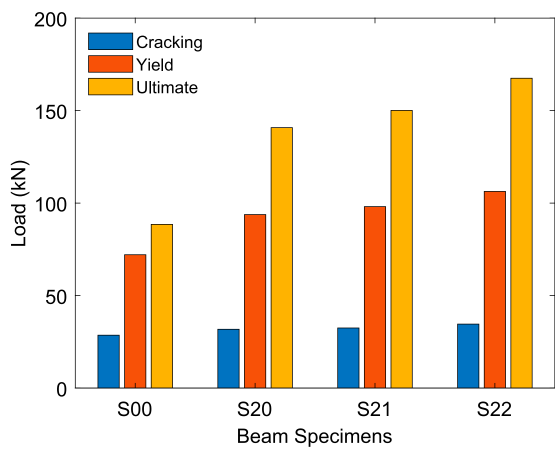

Figure 8. Summary of different types of loads in all specimens.

augmented section modulus of composite sections, resulting from the incorporation of a 40 mm mortar layer with a greater compressive strength, consequently leading to higher tensile strength as well. Furthermore, the prestressing of the concrete in the cases of S21 and S22 might also be an additional factor in the increase in crack initiation load. Cambering of the beam due to prestressing could be another reason for the increase in the crack initiation load of S21 and S22 (You et al., 2012). An additional load is required to reduce the upward deflection of the beam, which ultimately resulted in a further increase in the crack initiation load. Moreover, results from previous research were used for comparison and verification of the current study; the findings were found to be similar, in terms of the increase in crack initiation load due to the prestressing level, but they were different with respect to the types of strengthening materials used in the specimen, which included FRP rods, CFRP plates, FRP wraps, near surface mounted reinforcements and externally bonded sheets/laminates/plates (Badawi and Soudki, 2009; Hajihashemi et al., 2011; Nordin and Täljsten, 2006; Peng et al., 2014; Rashid et al., 2019; Woo et al., 2008; Xue et al., 2010; Yang et al., 2009; You et al., 2012).

The yield load and the ultimate load of beams show similar trends at higher values for strengthening and an even higher value for prestressing, as indicated in Figure 8. Beam S20 shows an increment of 30.10% in yield load compared to the control beam (S21 is 36.06% and S22 is 47.43%). The values for the ultimate loads are 59.10%, 69.60%, and 89.27% higher than the control specimen, respectively. It is also apparent that the yield load is 4.58% higher and the ultimate load is 6.61% higher when the prestressing level is 10%. The values increase to 13.33% and 18.96%, respectively, when the prestressing level is 20%, compared to the S20 beam, which was strengthened but not subjected to prestressing. Although the increase in prestressing level contributes to the increase in the crack initiation load, its impact is less significant than that of the yield load and ultimate load. Moreover, this study also analyzed the relationships between several types of loads and prestressing level, as suggested in Figure 9, and the relationship with the increase in ultimate load was observed to have produced a steep slope, yield load showed a decline, and cracking load showed a further decline when plotted. An increase in yield load and ultimate load, with the increase in the prestressing level, was also observed in many other studies in which different types of strengthening techniques were used (Badawi and Soudki, 2009; Hajihashemi et al., 2011; Nordin and Täljsten, 2006; Peng et al., 2014; Rashid et al., 2019; Woo et al., 2008; Xue et al., 2010; Yang et al., 2009; You et al., 2012), and this also verifies the current experimental observations.

Load-deflection relationships

Figure 10 shows the load-deflection curves for all types of beams, including control, strengthened, and prestressed strengthened, which indicates a tri-linear model related to beam behavior until failure. In the tri-linear model, the initial stiffness, crack initiation, and cracking moment are shown by the first slope, which is very steep. Meanwhile, the loading stages, from cracking to yield, are indicated by the second slope, which is less steep than the first due to the presence of higher loadings, and this caused more cracking. The third slope is the least steep and represents the loading from yield to the ultimate point. This slope, however, determines the beam ductility. The strengthening and prestressing cause a change in the initial stiffness. The prestressing creates compressive stresses on the beams and

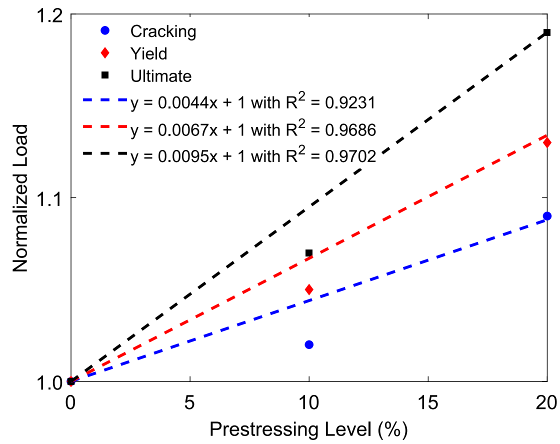

Figure 9. Influence of prestressing level on the flexural loads.

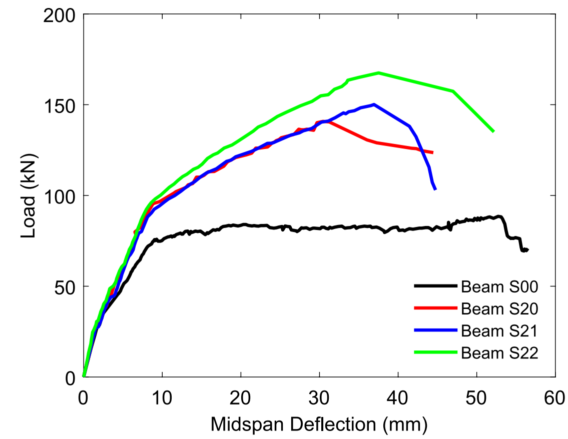

Figure 10. Load-midspan deflection curves of the tested beams.

the values increase with the increment in prestressing level. Furthermore, the conversion of these compressive stresses to tensile stresses leads to extra loading at the time of real loading; this causes larger beam deflection, as indicated by the 2.50% increase in the mid-span deflection at crack initiation load for S20, 16.00% for SS21, and 20.00% for SS22, compared to the control specimen.

The strengthened beams show higher values of yield load than the control beam, as previously explained, and they also have a moderately greater mid-span deflection when compared to the crack initiation load, due to strengthening and prestressing, as indicated by the second line of the tri-linear model. The mid-span deflection at yield load for S20 shows an increase of 4.88% (31.75% for S21 and 40.29% for S22) more than the un-strengthened beam. Moreover, the comparison between the prestressed and non-prestressed strengthened beam (S20) indicates that the mid-span deflection at ultimate load is enhanced by 19.55% and 23.26% at 10% and 20% prestressing levels, respectively.

Failure modes

Figure 11 depicts the typical failure modes for each beam specimen. The yielding of the steel rebar, followed by the crushing of concrete in the compression zone, was observed to have led to the failure of the control specimen. Meanwhile, as far as the constant moment region is concerned, the first appearance of flexural cracks is evident close to the mid-span, propagating deeply down the entire section from there, leading to ultimate failure. The first cracks are, therefore, observed at a load of 28.60 kN and this is followed by the appearance of several flexural cracks at 70.00 kN, which is almost identical to the yield load of the steel rebars. Ultimately, the cracks extend deeply down into the entire beam when the load is equal to 88.50 kN and this leads to the beam's failure. Each of the bonded prestressed-SWR-strengthened specimens shows the same flexural failure mode as the control beam, but they had different values for the initial cracking, yield load, and ultimate load capacity. Moreover, several flexural cracks are observed to have propagated deeply down the entire beam section, as well as some shear cracks between the support and loading point, but they were not responsible for the final beam failure. The same was also discovered for the debonding and separation of mortar covers.

Ductility index

The ductility of the beams in this study was evaluated using the ductility index, which is defined as the ratio of deflection at ultimate load to deflection at yield load (Haryanto et al., 2021d; Pamudji et al., 2021). A normalized ductility index is presented in Figure 12 and a reduction in the ductility index is observed with an increase in the prestressing level. The increase in tension reinforcement ratio and prestressing level, leading to reduced deflection at ultimate load, could potentially contribute to the decrease in ductility of strengthened beams. Another method to verify the phenomenon is by examining the studies conducted by other researchers, who utilized different types of strengthening techniques, such as external bonding or near-surface mounting (Rashid et al., 2019; Rezazadeh et al., 2014; Xue et al., 2010; Yang et al., 2009). In this study, the relationship between the ductility index and the prestressing level was further examined by regression analysis and a satisfactory coefficient of determination of 0.9827 was attained. It was concluded that a 10% increase in the prestressing level resulted in a 4% decrease in the ductility index, which is valid from zero to 20% prestressing levels.

Stiffness

Flexural stiffness (or rigidity) of the beam refers to its property of being able to resist bending or deflection when

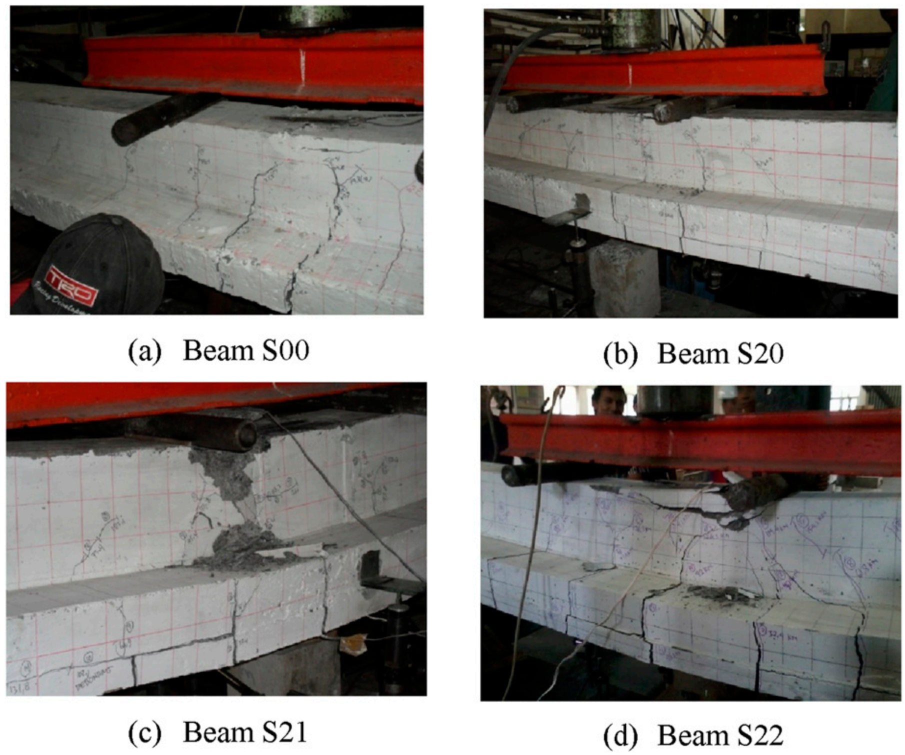

Figure 11. Failure modes of all types of beams.

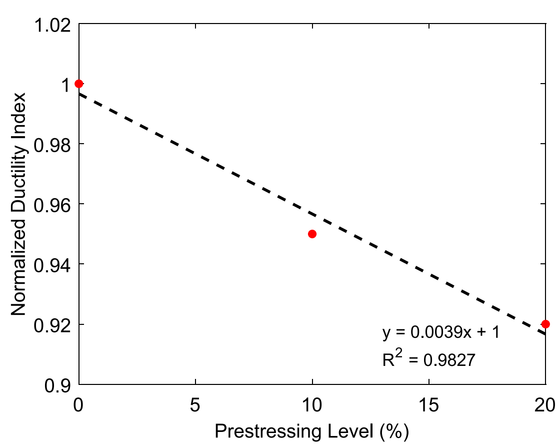

Figure 12. Influence of the prestressing level on the ductility of the negative-moment-region-bonded SWR-strengthened RC T-beams.

subjected to loading. It is a vital aspect of serviceability in concrete structures because higher stiffness causes changes in structural properties, such as deflection, ductility, and cracking behavior. It is, however, possible to use the load-deflection curves to determine the beam stiffness, as indicated in Figure 10. The initial stiffness of the beams is linear until the first crack appears. After the first crack, all specimens showed a reduction in stiffness. Most beams that carry service loads are usually at this stage (Nawy, 2005). This means that there is a need to evaluate the increment in beam stiffness in the service load range caused by the strengthening. The service load range is defined as the load range from the crack initiation load to the load corresponding to the point of deflection (equal to L/480, where L is the span length of the beam specimens). This ratio is provided by the ACI 318 standard (American Concrete Institute, 2019) for roofs or floors, constructed to support or be attached to nonstructural elements that are likely to be damaged by large deflections. In this study, the service load deflection (L/480) for the beam specimens was found to be 4.275 mm. The stiffness was calculated as the ratio of the applied load at the service range to the corresponding deflection. The stiffness values of all the specimens are presented in Figure 13.

Higher stiffness was observed for each beam subjected to strengthening under service loading, compared to the un-strengthened beam, and this was attributed to the pre-stressing of the bonded SWRs, as indicated by more stiffness at higher levels. The highest increase (52.55%), relative to the control beam, is shown by the strengthened beam which was subjected to a 20% prestressing level (S22). The stiffness and crack formation were, however, influenced by the internal steel reinforcement in the case of the regular un-strengthened beams (Qeshta et al., 2015). Meanwhile, the initiation and propagation of cracking in the strengthened beams were controlled by the strengthening material (Hosen et al., 2018; Obaydullah et al., 2016) and more so by the prestressing process, leading to higher stiffness. Hence, it can be said that the stiffness of the strengthened beam specimens in this study was directly related to the prestressing level of the strengthening materials.

Energy absorption capacities

One of the most important aspects related to the fracture evaluation of a structure is energy absorption (Qeshta et al., 2014). It is determined from the area under the curve obtained by plotting load against deflection and the values recorded for each specimen in this study are presented in Figure 14. The energy absorption capacity of the strengthened specimens can be seen to be greater than the control beam, and this is evident from the 13.80% higher value recorded for S20 (as well as 17.21% and 56.66% for SS21 and SS22, respectively). These higher capacities can be attributed to the delayed crack formation, higher stiffness, greater yield and ultimate load of these strengthened specimens. Moreover, the highest value was recorded with the specimen subjected to a prestressing level of 20%; this is possibly due to the significantly higher failure load and greater stiffness recorded after the yielding in the prestressed beams. It is, therefore, possible to conclude that a significantly higher energy absorption capacity is shown by the prestressed-SWR-strengthened beams. This is in line with the findings of previous studies: there is a higher energy absorption for prestressed strengthened beams with increments in the prestressing level, tensile steel ratio, or concrete compressive strength, provided that the concrete crushing controls the beam failure (Morais and Burgoyne, 2001; Omran and El-Hacha, 2010).

Concrete strain behavior

The compressive strain value recorded at the topmost fiber of the beam specimens is shown in Figure 15, with the control beam having 0.003440 as the maximum strain

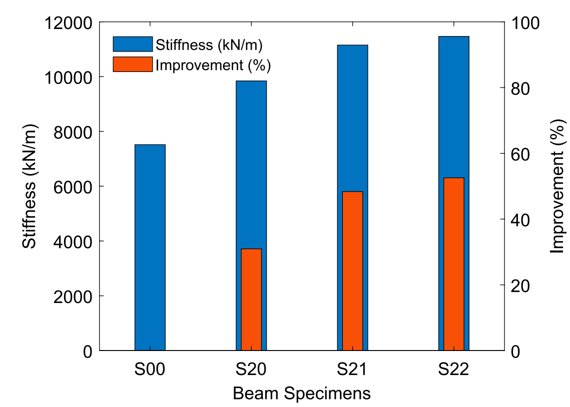

Figure 13. Improved stiffness of the strengthened specimens.

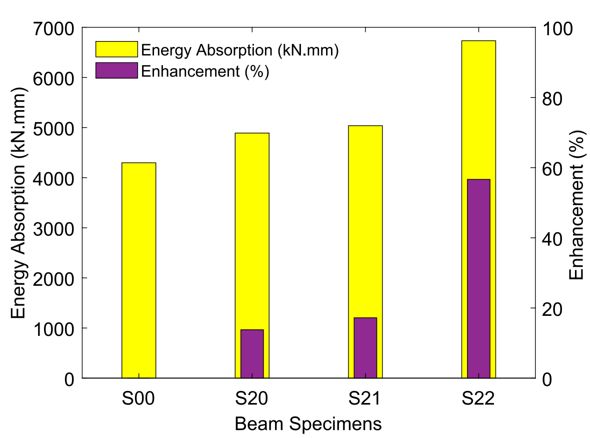

Figure 14. Energy absorption capacity of the specimens.

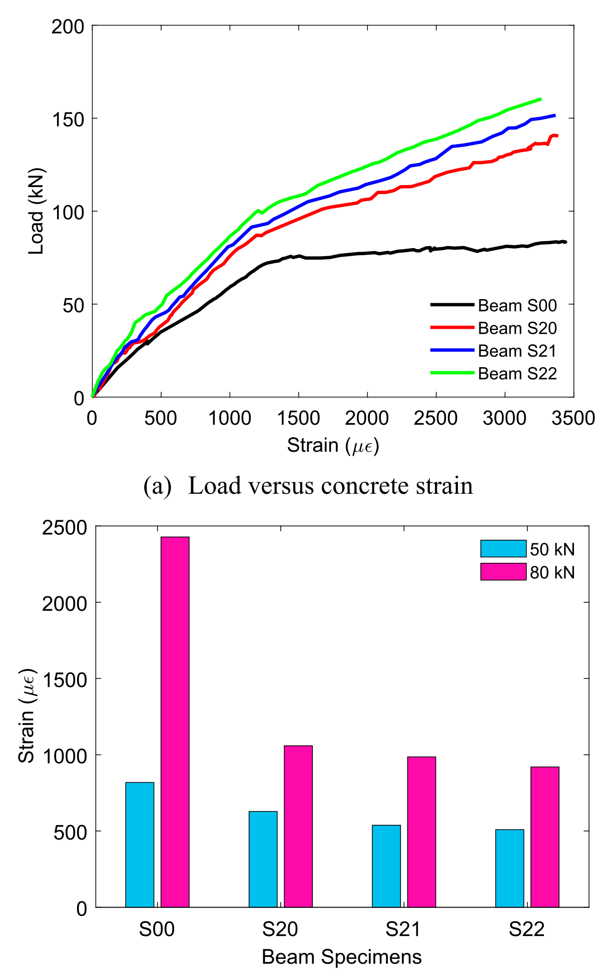

(a) Load versus concrete strain

(b) Concrete strain at 50 kN and 80 kN

Figure 15. Concrete compressive strain.

before concrete crushing. Prior to strain gauge damage, a value of maximum concrete compressive strain equal to 0.003387 was obtained for the non-prestressed SWR-strengthened beam (S20). In the case of the prestressed strengthened beams (S21 and S22), values equal to 0.003368 and 0.003266 were obtained. Moreover, Figure 13 indicates a decline in the value of concrete compressive strain due to an increment in the strengthening and prestressing levels. For example, a random load of 50 kN in Figure 13(b) shows declines of 23.23%, 34.23%, and 37.78% in the concrete compressive strains for specimens subjected to prestressing levels of 0%, 10%, and 20%, respectively. Similarly, another high random load of 80 kN showed a similar trend, with the concrete compressive strain observed to be declining as the specimens were subjected to further strengthening and prestressing. This is associated with the increment in stiffness due to strengthening, thereby reducing the value of concrete compressive strain over the topmost fiber of the beam.

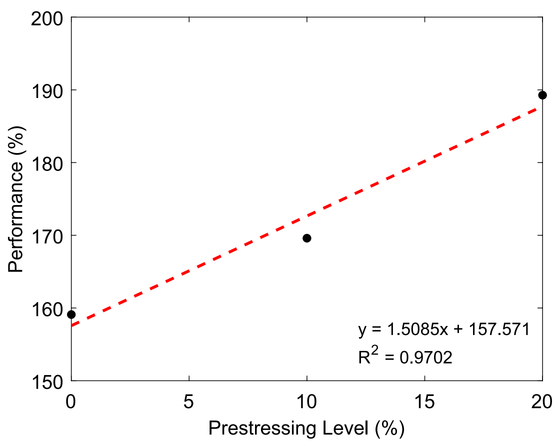

Figure 16. Influence of the prestressing level on the flexural performance of negative-moment-region-bonded SWR-strengthened RC T-beams.

Table 3. Predicted FLexural performance.

	Flexural performance (%)	
Specimen	Experimental	Predicted
S20	159.10	157.57
S21	169.60	172.66
S22	189.27	187.74

Efficiency of the strengthening technique

The efficiency of the strengthening technique applied in this study was controlled by the level of prestressing force in the SWRs, which was found to be directly and positively related to the flexural performance demonstrated in Figure 16. This means that any increment in the prestressing force was observed to have led to a significant increment in the negative moment region flexural performance of RC T-beam specimens, the maximum being recorded at approximately 189.27%. This relationship is represented by the following equation, with a coefficient of determination of 0.9702:

$$F = 1.5085P_s + 157.571 \tag{1}$$

where F is flexural performance (%) and P_s is the prestress level of SWRs (%). The observed and predicted values of flexural performance of the strengthened specimens with

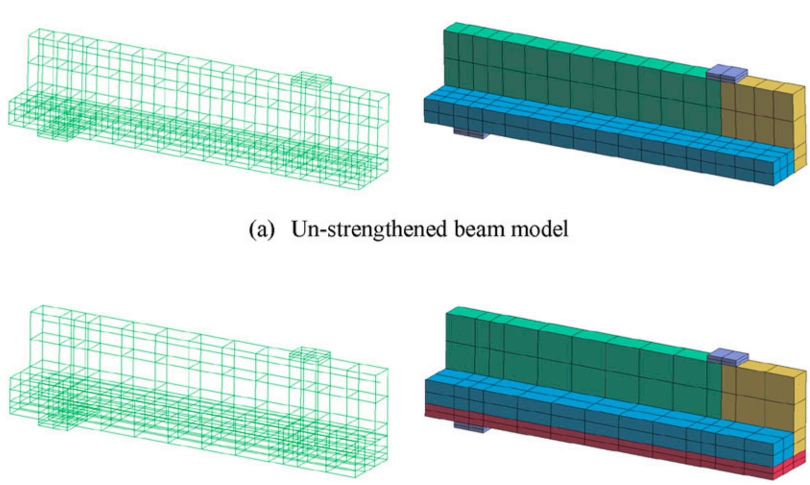

(a) Un-strengthened beam model

(b) Strengthened beam model

Figure 17. FE model of tested beams.

prestressed bonded SWRs are compared in Table 3. The values were obtained by inserting the prestressing level of SWRs as the strengthening material in equation (1) and the results show a close variance between the values.

Finite element model

Finite element (FE) software ATENA (Cervenka et al., 2021) was used to develop the 3D FE model in this work. This program has a history of providing reliable outcomes close to experimental values (Haryanto et al., 2017b; Hidayat et al., 2019; Jirawattanasomkul et al., 2018). The model demonstrates congruence with the beam specimen that underwent testing, in relation to its geometric properties, material properties, and boundary conditions. Because the parameters are consistent, a fractional representation of each beam, namely one fourth, was used for modeling. As stated by Zheng et al. (2020), a numerical convergence investigation demonstrated that decreasing the mesh size in the FE analysis (FEA) had minimal effect on the numerical outcome but substantially increased the computation time. Thus, in order to optimize computational efficiency and minimize runtime in this study, the FEA utilized structured meshes consisting of three linear elements and 200 hexahedral elements for the un-strengthened beam model, along with three linear elements and 198 hexahedral elements for the strengthened beam model, as shown in Figure 17. The material models and the selection of element types that were applied to the 3D models are explained in subsequent sections.

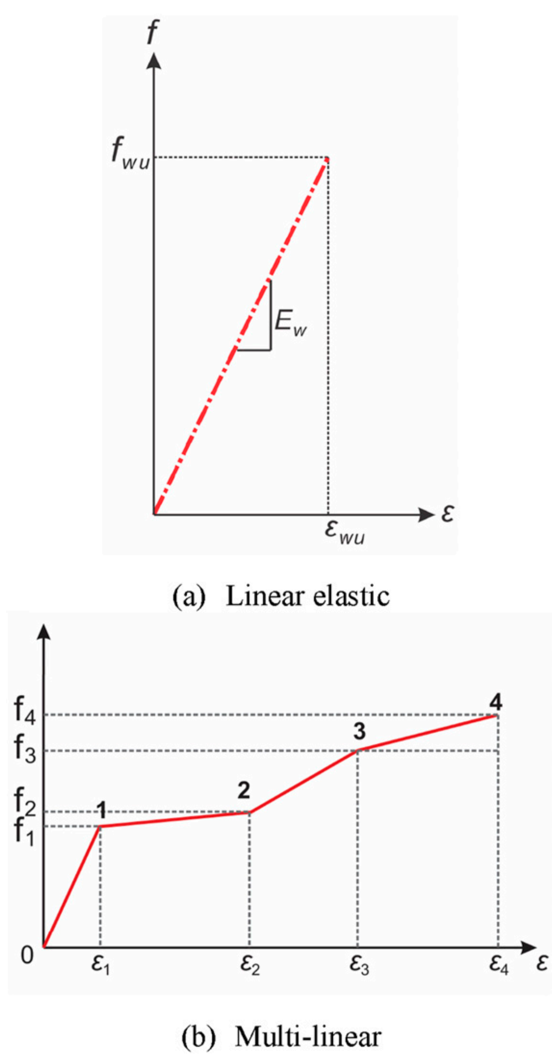

Figure 18. Stress–strain law for SWR and steel reinforcement.

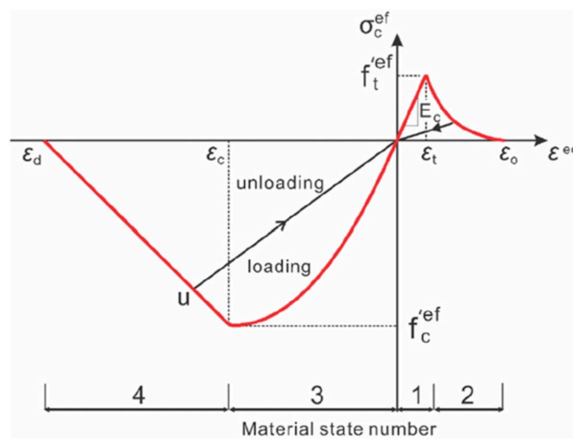

Figure 19. Uniaxial stress–strain law for concrete.

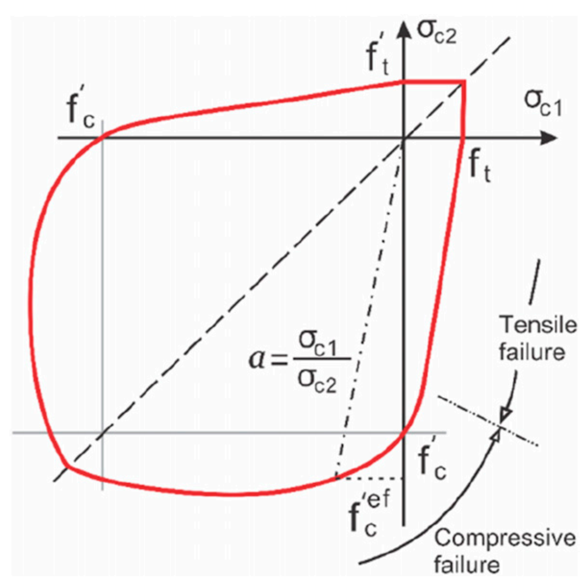

Figure 20. Biaxial failure function for concrete.

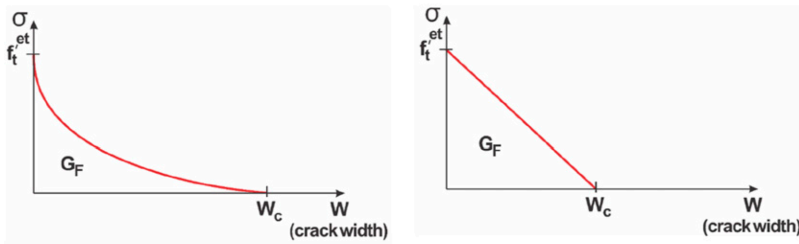

(a) Exponential (b) Linear

Figure 21. Crack-opening laws.

Material modeling

Figure 18 demonstrates that SWRs exhibit tensile behavior with a linearly elastic stress-strain relationship up to the point of failure, whereas the steel reinforcement constitutive model was established by applying a multi-linear law. This law allows the modeling of all four stages of steel behavior: elastic state, yield plateau, hardening and fracture. The multi-line is defined by four points, which can be specified by input. Meanwhile, the smeared cracking property and the fracture mechanics approach served as the basis for the development of basic constitutive models for the concrete in the ATENA software, due to its non-linear and heterogeneous structure. Moreover, the concept of fracturing derived from the uniaxial stress-strain law explains the prevailing stress reaction, which means the monotonic loading led to concrete fracture, as presented in Figure 19. Based on the recommendation by Kupfer et al. (1969), the peak stress under uniaxial behavior ($f_t'^{ef}$ and $f_c'^{ef}$) was estimated in the biaxial failure surface depicted in Figure 20. In addition, a simulated crack model was utilized to analyze the stress response of concrete. This model was generated using the crack-opening law and fractural energy, incorporating the crack band theory (Bažant and Lin, 1988; Bažant and Oh, 1983). The purpose of this was to address two limitations associated with the use of the FE model: the element size effect and the element orientation effect.

Figure 21 illustrates that ATENA software uses an exponential function derived from Hordijk's study of the exponential crack-opening law (Hordijk, 1991), along with a linear crack-opening law. It also assumes a simulated compression model from van Mier's study (van Mier, 1986), in the case of the compression following the peak stress with the tension failure deemed to be restricted in the plane located perpendicular to the principal stress direction, as depicted in Figure 22. Moreover, Figure 23 indicates that ATENA has two crack models, which include fixed and rotated cracks, such that the direction of cracking and the principal strain are parallel to each other in the fixed crack models. This direction, however, changes with the strain direction.

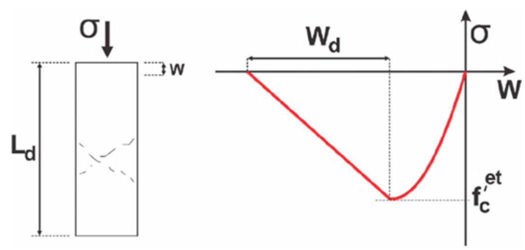

Figure 22. Softening displacement law in compression.

Element selection

A perfect bond is presumed to be present in each material. Table 4 displays the types of elements employed for modeling in this study. The concrete and mortar were modeled using CC3DnonLinCementitious2, which is a solid element characterized by eight nodes. This material is suitable for use in creep measurements since it involves the presumption of a hardening regime before the attainment of compressive strength. It is also applicable when the material properties need modification at some point in the analysis. Meanwhile, CCReinforcement elements, characterized by two nodes, were used to model the longitudinal reinforcements as well as the SWRs. These elements have the ability to disable the reinforcements' compressive response and are very useful when used to simulate the reinforcement behavior of a material characterized by lower bending stiffness, such as SWR. This is because it can be assumed that the occurrence of buckling occurs in such a case and that the strength of the elements in compression is negligible when the reinforcement material is subjected to compressive forces. Furthermore, a solid material known as CC3DElastIsotropic, which is characterized by eight nodes, was also applied to model the loading and the supporting plates used for the 3D simulation of linear isotropic materials. An eight-node CCCombinedMaterial element was applied to model the concrete with stirrups, due to its potential to form a complex compound in multiple directions, such as a combination of concrete and smeared reinforcement.

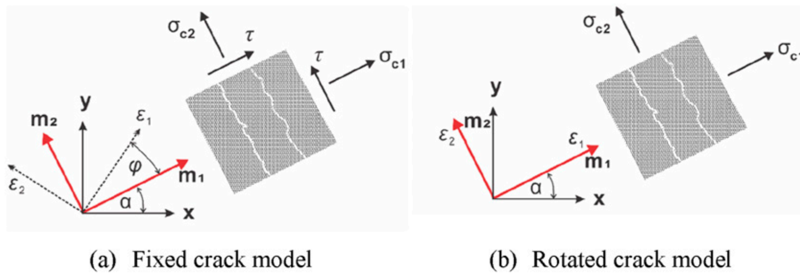

Figure 23. Two models of smeared cracks.

Table 4. Materials and types of elements.

Materials	Element type	Properties	Data
Concrete	*CC3DnonLinCementitous2*	Compression strength	32.39
		Young's modulus, E_c	27,545.489
Mortar	*CC3DnonLinCementitous2*	Compression strength	49.85
		Young's modulus, E_c	30,025.891
Reinforcement P8	*CCReinforcement*	Young's modulus, E_s	201,640.000
		Ultimate stress, f_u	525.33
		Yield stress, f_y	373.85
		Area of reinforcement, *A*	0.00005024
Reinforcement D13	*CCReinforcement*	Young's modulus, E_s	197,660.000
		Ultimate stress, f_u	742.52
		Yield stress, f_y	479.71
		Area of reinforcement, *A*	0.000132665
Steel wire rope P10	*CCReinforcement*	Young's modulus, E_s	132,570.000
		Ultimate stress, f_u	743.73
		Yield stress, f_y	-
		Area of reinforcement, *A*	0.00007850
Concrete stirrup P8-40	*CCCombinedMaterial*	Area of shear reinforcment, A_v	0.00080380
		Ratio of direction x reinforcement (1)	0.0032154
		Ratio of direction y reinforcement (2)	0.0053589
		Ratio of direction z reinforcement (3)	0
Concrete stirrup P8-100	*CCCombinedMaterial*	Area of shear reinforcment, A_v	0.0003517
		Ratio of direction x reinforcement (1)	0.0014067
		Ratio of direction y reinforcement (2)	0.0023445
		Ratio of direction z reinforcement (3)	0
Loading and support plates	*CC3DElastIsotropic*	Young's modulus, E_s	200,000.000
		Poisson's ratio, *v*	0.3

Model validation

Model validation is essential, in order to confirm the accuracy and reliability of theoretical and FE analyses by comparing model results with experimental data, highlighting limitations and improving modeling techniques (Li et al., 2022; Rashedi et al., 2022; Sun et al., 2024; Tang et al., 2024; Zhang et al., 2022). This process builds confidence in the model's predictions, supports design optimization, and ensures compliance with regulatory standards. In this paper, the developed FE models were validated and verified using the experimental findings for the load and midspan deflections. It is worth mentioning that a previous study by Haryanto et al. (2017a) also provided further details on these modeling results. The curve plotted for load against midspan deflection at each loading stage before ultimate failure was predicted for each specimen, as indicated in Figure 24. The FE modeling curves exhibit a high level of agreement with the experimental data. The FE simulation successfully predicts the peak load of the beams. Furthermore, the FE simulation accurately replicates the overall varying trends observed in the load-deflection curves for all beams. However, the FE model produced slightly higher stiffness, which is

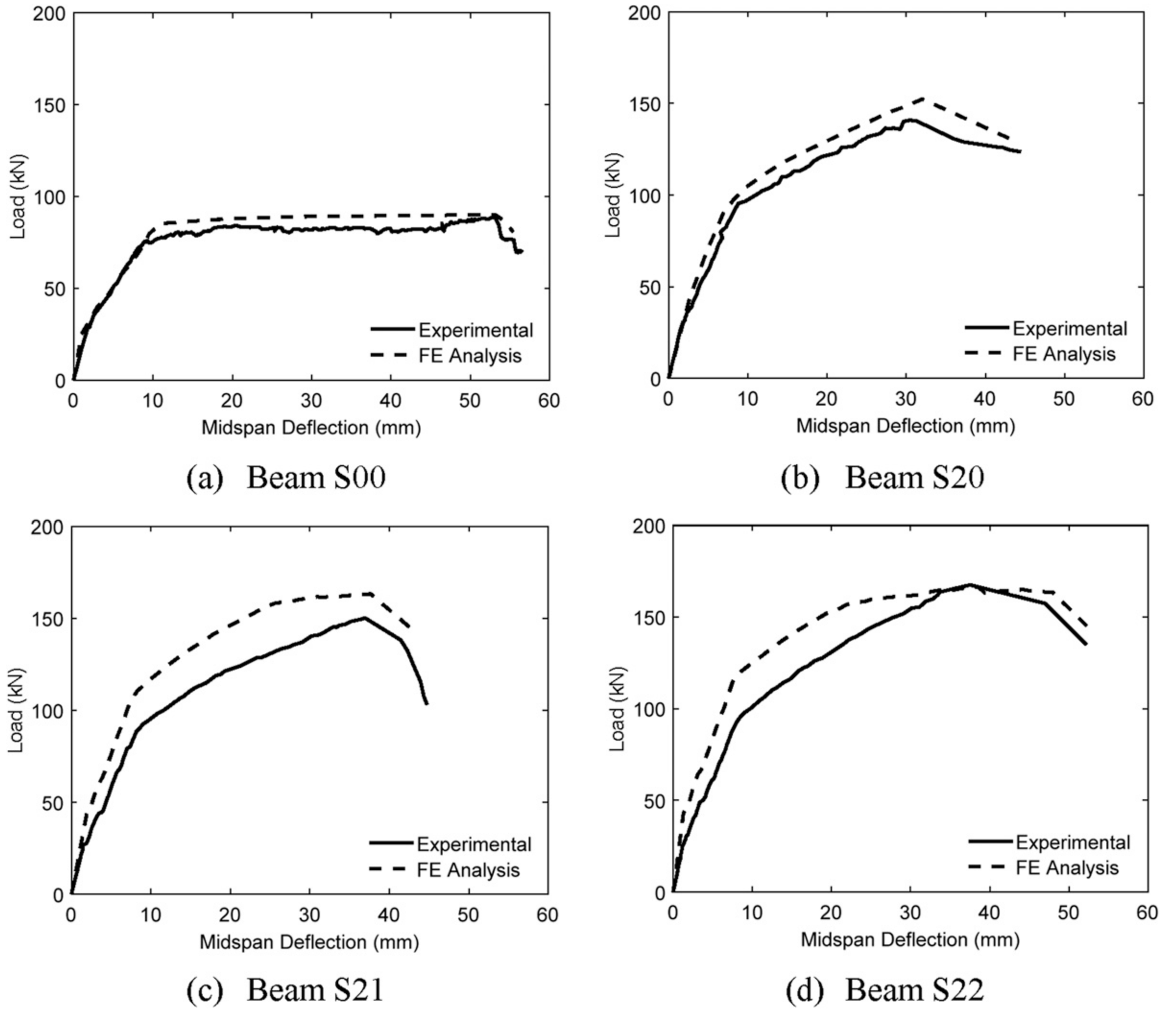

Figure 24. Load–deflection curve comparisons between FE models and experimental results.

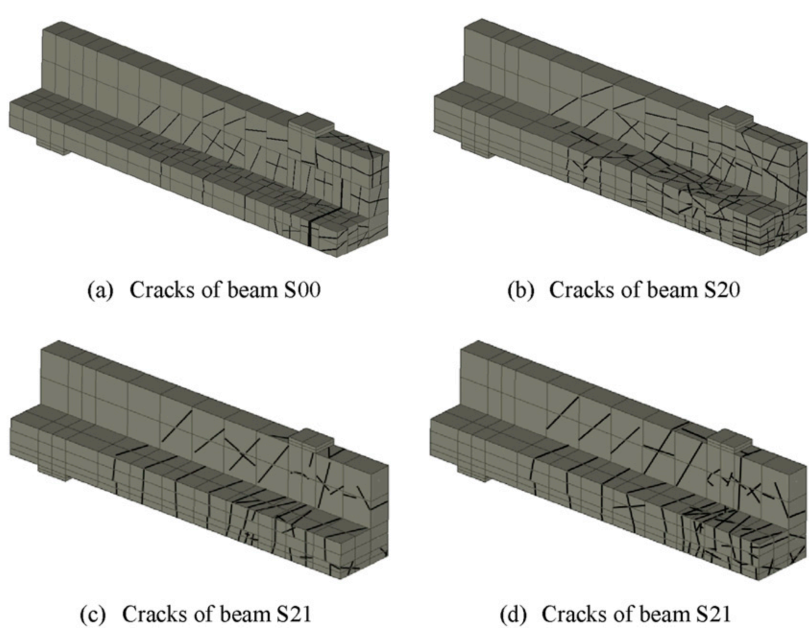

Figure 25. Simulated crack patterns at failure.

Table 5. FE analysis versus experimental results.

Specimens	Ultimate load P_u (kN)		Corresponding deflection δ_u (mm)		Percentage difference (%)	
	FE analysis	Experimental	FE analysis	Experimental	P_u	δ_u
S00	90.00	88.50	53.14	52.72	1.7	0.8
S20	152.38	140.80	32.05	30.44	8.2	5.3
S21	163.18	150.10	37.65	36.39	8.7	3.5
S22	166.57	167.50	37.95	37.52	0.6	1.1

associated with the assumption of a perfect bond between the steel and concrete, as well as SWR and mortar. These bonds neglect the bond-slip relationship and this leads to an increment in the beam's flexural stiffness, thereby causing an overestimation of the strain concentration in steel at the crack locations. Figure 25 illustrates the failure modes observed at the point of failure, as determined through the FE simulation. The findings of the FE simulation exhibit good agreement with the experimental test results. This is evident from the identified crack patterns and their propagation from the bottom to the top, which indicate that all models experienced flexural failure.

In order to provide additional evidence of the accuracy of the developed finite element (FE) model, the ultimate load and corresponding midspan deflections were extracted from the FE simulation. These values were then compared with the relevant experimental results, which are listed in Table 5. The FE results demonstrate a high level of accuracy, in terms of both the ultimate load and the corresponding midspan deflection. The predictions for ultimate load had an approximately 0.5%–9.0% disparity, while those for the corresponding deflection were between 0.5% and 5.5% of the experimental values. Therefore, the FE model demonstrated its precision in predicting the characteristics and performance of RC T-beams strengthened with bonded prestressed SWRs in the region of negative bending moments. This means that the model is appropriate to be applied by engineers and researchers examining several factors affecting the behavior of strengthened and prestressed beams.

Conclusions

This research was conducted to explore the flexural performance of RC T-beams, strengthened using bonded SWRs in the negative moment region at different prestressing levels. Therefore, three beam specimens were made with bonded SWRs, of which two were subjected to a prestressing level of 10% or 20% of the tensile strength of SWR, along with a control beam. The parameters measured through four-point bending tests include the cracking load, yield load, ultimate load, and mid-span deflection, after which the results from the experiment were verified numerically and this led to the following conclusions:

1) The flexural strengthening of RC T-beams in the negative moment region using pre-stressed SWRs proved to be effective, as indicated by the enhancement in the crack initiation load, yield load, and ultimate load of beams S20, S21, and S22 (by 10%–30%, 30%–50%, and 50%–90%, respectively).
2) The topmost fiber in each strengthened beam experienced concrete crushing and this led to the flexure failure. This is a highly anticipated failure mode in strengthened beams, just like in the control specimen. Meanwhile, shear cracks, debonding, and separation of mortar cover were observed in the strengthened beams, but they were not responsible for the final failure.
3) A linear relationship between the ductility index and the pre-stressing level was established with a coefficient of determination of 0.9827; it was concluded that a 4% reduction in the ductility index was observed with a 10% increase in the prestressing level. This trend was valid from 0 to 20% of the prestressing level.
4) A significant increase in the stiffness of the beams strengthened with bonded prestressed SWRs was observed under service loading, with the highest increase (52.55%) shown by the beam with a 20% prestress level (S22).
5) The energy absorption capacity of all strengthened specimens exceeded that of the control beam. Specifically, S20 showed a 13.80% increase, SS21 exhibited a 17.21% increase, and SS22 demonstrated the highest increase at 56.66%.
6) While the FE model assumed perfect bonding, actual bond-slip behavior introduces variability. This necessitates further research to better represent bond-slip behavior in bonded-prestressed-SWR-strengthened RC T-beams. Comprehensive parametric studies are needed to explore a wider range of variables and conditions.

Acknowledgments

The authors would like to express their gratitude to the Institute for Research and Community Service, Jenderal Soedirman University UNSOED), Indonesia, for their financial sponsorship of the experimental investigation (3747/UN23.14/PN/2018) and the numerical study (26.414/UN23.35.5/PT.01/II/2024). We also acknowledge the partial support provided by Diponegoro University (UNDIP), Indonesia, through the World Class University program (123/UN7. A/HK/XII/2023). The efforts of Pandu Suliwandanu, Muhammad Farid Risqullah, and Adrianus Alma Setiawan, with respect to modeling, are also appreciated.

Declaration of conflicting interests

The author(s) declared no potential conflicts of interest with respect to the research, authorship, and/or publication of this article.

Funding

The author(s) disclosed receipt of the following financial support for the research, authorship, and/or publication of this article: This work was supported by Jenderal Soedirman University; 3747/UN23.14/PN/2018, Diponegoro University; 123/UN7.A/HK/XII/2023, Jenderal Soedirman University; 26.414/UN23.35.5/PT.01/II/2024.

ORCID iDs

Yanuar Haryanto https://orcid.org/0000-0002-5322-7503
Laurencius Nugroho https://orcid.org/0000-0003-1956-3009
Hsuan-Teh Hu https://orcid.org/0000-0001-8582-0670

References

Abdalla JA, Abu-Obeidah AS, Hawileh RA, et al. (2016) Shear strengthening of reinforced concrete beams using externally bonded aluminum alloy plates: an experimental study. *Construction and Building Materials* 128: 24–37.

Abu-Obeidah A, Hawileh RA and Abdalla JA (2015) Finite element analysis of strengthened RC beams in shear with aluminum plates. *Computers & Structures* 147: 36–46.

Abuodeh OR, Abdalla JA and Hawileh RA (2020) Prediction of shear strength and behavior of RC beams strengthened with externally bonded FRP sheets using machine learning techniques. *Composite Structures* 234: 111698.

ACI 318-19 (2019) *Building Code Requirements for Structural Concrete*.Farmington Hills, MI: American Concrete Institute.

Al-Khafaji A and Salim H (2020) Flexural strengthening of RC continuous T-beams using CFRP. *Fibers* 8(6): 41.

Al-Rousan RZ (2017) Shear behavior of RC beams externally strengthened and anchored with CFRP composites. *Structural Engineering and Mechanics* 63(4): 447–456.

Amran YHM, Alyousef R, Rashid RSM, et al. (2018) Properties and applications of FRP in strengthening RC structures: a review. *Structures* 16: 208–238.

ASTM A370-18 (2018) *Standard Test Methods and Definitions for Mechanical Testing of Steel Products*. West Conshohocken, PA: ASTM International.

ASTM C109/C109M-20 (2020) *Standard Test Method for Compressive Strength of Hydraulic Cement Mortars (Using 2-in. Or [50-mm] Cube Specimens)*. West Conshohocken, PA: ASTM International.

ASTM C39/C39M-21 (2021) *Standard Test Method for Compressive Strength of Cylindrical Concrete Specimens*. West Conshohocken, PA: ASTM International.

Attari N, Youcef YS and Amziane S (2019) Seismic performance of reinforced concrete beam–column joint strengthening by FRP sheets. *Structures* 20: 353–364.

Badawi M and Soudki K (2009) Flexural strengthening of RC beams with prestressed NSM CFRP rods - experimental and analytical investigation. *Construction and Building Materials* 23(10): 3292–3300.

Bažant ZP and Lin FB (1988) Nonlocal smeared cracking model for concrete fracture. *Journal of Structural Engineering* 114(11): 2493–2510.

Bažant ZP and Oh BH (1983) Crack band theory for fracture of concrete. *Matériaux et Constructions* 16(3): 155–177.

Bencardino F, Colotti V, Spadea G, et al. (2006) Holistic design of RC beams and slabs strengthened with externally bonded FRP laminates. *Cement and Concrete Composites* 28: 832–844.

Cervenka V, Cervenka J, Janda Z, et al. (2021) *ATENA Program Documentation Part 8; User's Manual for ATENA-GiD Interface*. Prague: Cervenka Consulting.

Choobbor SS, Hawileh RA, Abu-Obeidah AS, et al. (2019) Performance of hybrid carbon and basalt FRP sheets in strengthening concrete beams in flexure. *Composite Structures* 227: 111337.

Demir A, Ercan E and Demir DD (2018) Strengthening of reinforced concrete beams using external steel members. *Steel and Composite Structures* 27(4): 453–464.

Fayed S, Basha A and Hamoda A (2019) Shear strengthening of RC beams using aluminum plates: an experimental work. *Construction and Building Materials* 221: 122–138.

Firmo JP, Correia JR and Bisby LA (2015) Fire behaviour of FRP-strengthened reinforced concrete structural elements: a state-of-the-art review. *Composites Part B: Engineering* 80: 198–216.

Fontanari V, Benedetti M, Monelli B, et al. (2015) Fire behavior of steel wire ropes: experimental investigation and numerical analysis. *Engineering Structures* 84: 340–349.

Franco N, Biscaia H and Chastre C (2018) Experimental and numerical analyses of flexurally-strengthened concrete T-beams with stainless steel. *Engineering Structures* 172: 981–996.

Grace NF (2001) Strengthening of negative moment region of reinforced concrete beams using carbon fiber-reinforced polymer strips. *ACI Structural Journal* 98(3): 347–358.

Gudonis E, Timinskas E, Gribniak V, et al. (2014) FRP reinforcement for concrete structures: state-of-the-art review of application and design. *Engineering Structures and Technologies* 5: 147–158.

Hajihashemi A, Mostofinejad D and Azhari M (2011) Investigation of RC beams strengthened with prestressed NSM CFRP laminates. *Journal of Composites for Construction* 15(6): 887–895.

Han AL, Hu H-T, Gan BS, et al. (2022) Carbon fiber-reinforced polymer rod embedment depth influence on concrete strengthening. *Arabian Journal for Science and Engineering* 47: 12685–12695.

Haryanto Y, Gan BS and Maryoto A (2017a) Wire rope flexural bonded strengthening system on RC-beams: a finite element simulation. *International Journal of Technology* 8(1): 132–144.

Haryanto Y, Gan BS, Widyaningrum A, et al. (2017b) Near surface mounted bamboo reinforcement for flexural strengthening of reinforced concrete beams. *Jurnal Teknologi* 79(6): 233–240.

Haryanto Y, Gan BS, Widyaningrum A, et al. (2018) On the performance of steel wire rope as the external strengthening of RC beams with different end-anchor type. *Jurnal Teknologi* 80(5): 145–154.

Haryanto Y, Hu H-T, Han AL, et al. (2019) Finite element analysis of T-section RC beams strengthened by wire rope in the negative moment region with an addition of steel rebar at the compression block. *Jurnal Teknologi* 81(4): 143–154.

Haryanto Y, Hu H-T, Han AL, et al. (2021b) Negative moment region flexural strengthening system of RC T-beams with half-embedded NSM FRP rods: a parametric analytical approach. *Journal of the Chinese Institute of Engineers* 44(6): 553–561.

Haryanto Y, Hu H-T, Han AL, et al. (2021c) Nonlinear 3D model of double shear lap tests for the bond of near-surface mounted FRP rods in concrete considering different embedment depth. *Periodica Polytechnica: Civil Engineering* 65(3): 878–889.

Haryanto Y, Hu H-T, Han AL, et al. (2021d) Numerical investigation on RC T-beams strengthened in the negative moment region using NSM FRP rods at various depth of embedment. *Computers and Concrete* 28(4): 347–360.

Haryanto Y, Han AL, Hu H-T, et al. (2021a) Enhancement of flexural performance of RC beams with steel wire rope by external strengthening technique. *Journal of the Chinese Institute of Engineers* 44(3): 193–203.

Haryanto Y, Hsiao F-P, Hu H-T, et al. (2022) Structural behavior of negative moment region NSM-CFRP strengthened RC T-beams with various embedment depth under monotonic and cyclic loading. *Composite Structures* 301: 116214.

Haryanto Y, Hsiao F-P, Hu H-T, et al. (2023) Validating an analytical method to predict flexural behavior of RC T-beams retrofitted with bonded steel wire ropes in the negative moment region. *AIP Conference Proceedings* 2482(1): 030001.

Haryanto Y, Hu H-T, Han AL, et al. (2021e) Numerical parametric study on the flexural capacity of reinforced concrete beams strengthened with non-metallic materials. *Journal of Engineering Science & Technology* 16(4): 3295–3311.

Hidayat BA, Hu H-T, Han AL, et al. (2019) Nonlinear finite element analysis of traditional flexural strengthening using betung bamboo (dendrocalamus asper) on concrete beams. *IOP Conference Series: Materials Science and Engineering* 615: 012073.

Hordijk DA (1991) *Local Approach to Fatigue of Concrete*. Netherlands: Delft University of Technology. Ph.D. Dissertation.

Hosen MA, Jumaat MZ, Alengaram UJ, et al. (2018) CFRP strips for enhancing flexural performance of RC beams by SNSM strengthening technique. *Construction and Building Materials* 165: 28–44.

Hosen MA, Jumaat MZ, Darain KMU, et al. (2014) Flexural strengthening of RC beams with NSM steel bars. *International Conference on Food, Agriculture and Biology (FAB-2014)*. Kuala Lumpur, Malaysia, 11-12 June 2014.

Hung C-C, El-Tawil S and Chao S-H (2021) A review of developments and challenges for UHPC in structural engineering: behavior, analysis, and design. *Journal of Structural Engineering* 147(9): 1–19.

Hung C-C, Hsiao H-J, Shao Y, et al. (2023) A comparative study on the seismic performance of RC beam-column joints retrofitted by ECC, FRP, and concrete jacketing methods. *Journal of Building Engineering* 64: 105691.

Hussain HK, Zhang LZ and Liu GW (2013) An experimental study on strengthening reinforced concrete T-beams using new material poly-urethane-cement (PUC). *Construction and Building Materials* 40: 104–117.

Ism MM and Rabie M (2019) Flexural behavior of continuous RC beams strengthened with externally bonded CFRP sheets. *Alexandria Engineering Journal* 58: 789–800.

JGJ/T 325-2014 (2014) *Technical Specifcation for Strengthening Concrete Structures with Prestressed High Strength Steel Wire Ropes [in Chienese]*. Beijing, China: Ministry of Housing and Urban-Rural Development of China.

Jirawattanasomkul T, Kongwang N, Jongvivatsakul P, et al. (2018) Finite element modelling of fexural behaviour of geosynthetic cementitious composite mat (GCCM). *Composites Part B: Engineering* 154: 33–42.

Jones R, Swamy R and Charif A (1988) Plate separation and anchorage of reinforced concrete beams strengthened by epoxy-bonded steel plates. *Structural Engineer* 66(5): 85–94.

Jumaat MZ, Rahman MM and Alam MA (2010) Flexural strengthening of RC continuous T beam using CFRP laminate: a review. *International Journal of the Physical Sciences* 5(6): 619–625.

Kim SY, Yang KH, Byun HY, et al. (2007) Tests of reinforced concrete beams strengthened with wire rope units. *Engineering Structures* 29: 2711–2722.

Kupfer H, Hilsdorf HK and Rüsch H (1969) Behavior of concrete under biaxial stresses. *ACI Journal Proceedings* 66(8): 656–666.

Lampropoulos AP, Paschalis SA, Tsioulou OT, et al. (2016) Strengthening of reinforced concrete beams using ultra high performance fibre reinforced concrete (UHPFRC). *Engineering Structures* 106: 370–384.

Lee WK (1991) An insight into wire rope geometry. *International Journal of Solids and Structures* 28(4): 471–490.

Lee DH, Han SJ, Kim KS, et al. (2017) Shear strength of reinforced concrete beams strengthened in shear using externally-bonded FRP composites. *Composite Structures* 173: 177–187.

Lesmana C and Hu H-T (2014) Parametric analyses of square reinforced concrete slabs strengthened by fiber-reinforced plastics. *Construction and Building Materials* 53: 294–304.

Lesmana C and Hu H-T (2015) Nonlinear finite element analysis of rectangular reinforced concrete slabs strengthened by reinforced plastics. *Scientia Iranica* 22(3): 615–628.

Lesmana C, Hu H-T, Lin F-M, et al. (2013) Numerical analysis of square reinforced concrete plates strengthened by fiber-reinforced plastics with various patterns. *Composites Part B: Engineering* 55: 247–262.

Li X, Wu G, Shafiq Popal M, et al. (2018) Experimental and numerical study of hollow core slabs strengthened with mounted steel bars and prestressed steel wire ropes. *Construction and Building Materials* 188: 456–469.

Li H, Li L, Fan X, et al. (2022) Experimental and numerical investigation on the flexural behavior of a large-scale prestressed UHPC T-Shaped girder. *Engineering Structures* 272: 115027.

MacDonald M and Calder AJJ (1982) Bonded steel plating for strengthening concrete structures. *International Journal of Adhesion and Adhesives* 2(2): 119–127.

Morais M and Burgoyne C (2001) Energy Dissipation in Sections Prestressed with FRP Tendons. *The International Conference on Composites in Construction (CCC 2001)*. Porto, Portugal, 10-12 October 2001.

Mukhtar FM and Faysal RM (2018) A review of test methods for studying the FRP-concrete interfacial bond behavior. *Construction and Building Materials* 169: 877–887.

Nahar TT and Rahman MM (2015) Strengthening of RCC beams using bamboo sticks. *International Journal of Advanced Science and Technology* 79: 15–24.

Nawy EG (2005) *Reinforced Concrete a Fundamental Approach*. Hoboken, NJ: Prentice Hall.

Nordin H and Täljsten B (2006) Concrete beams strengthened with prestressed near surface mounted CFRP. *Journal of Composites for Construction* 10(1): 60–68.

Obaydullah M, Jumaat MZ, Alengaram UJ, et al. (2016) Prestressing of NSM steel strands to enhance the structural performance of prestressed concrete beams. *Construction and Building Materials* 129: 289–301.

Oller E, Pujol M and Marí A (2019) Contribution of externally bonded FRP shear reinforcement to the shear strength of RC beams. *Composites Part B: Engineering* 164: 235–248.

Omran H and El-Hacha R (2010) Parametric study of RC girders strengthened in flexure using prestressed NSM CFRP strips. *International Conference on Seismic Retrofitting of Structures (ICSR2010)*. Tabriz, Iran, 20-22 Ocotber 2010.

Pamudji G, Haryanto Y, Hu H-T, et al. (2021) The flexural behavior of RC beams with sand-coated polypropylene waste coarse aggregate at different w/c ratios. *Advances in Materials Research* 10(4): 313–329.

Papanicolaou CG, Triantafillou TC, Papathanasiou M, et al. (2007) Textile reinforced mortar TRM versus FRP as strengthening material of URM walls: out-of-plane cyclic loading. *Materials and Structures* 41(1): 143–157.

Peled A (2007) Confinement of damaged and nondamaged structural concrete with FRP and TRC sleeves. *Journal of Composites for Construction* 11(5): 514–522.

Peng H, Zhang J, Cai CS, et al. (2014) An experimental study on reinforced concrete beams strengthened with prestressed near surface mounted CFRP strips. *Engineering Structures* 79: 222–233.

Qasim M, Lee C and Zhang Y (2023) Flexural strengthening of reinforced concrete beams using hybrid fibre reinforced engineered cementitious composite. *Engineering Structures* 284: 115992.

Qeshta IMI, Shafigh P, Jumaat MZ, et al. (2014) The use of wire mesh-epoxy composite for enhancing the ;exural performance of concrete beams. *Materials & Design* 60: 250–259.

Qeshta IMI, Shafigh P and Jumaat MZ (2015) Flexural behaviour of RC beams strengthened with wire mesh-epoxy composite. *Construction and Building Materials* 79: 104–114.

Qeshta IMI, Shafigh P and Jumaat MZ (2016) Research progress on the flexural behaviour of externally bonded RC beams. *Archives of Civil and Mechanical Engineering* 16: 982–1003.

Raithby KD (1982) Strengthening of concrete bridge decks with epoxy-bonded steel plates. *International Journal of Adhesion and Adhesives* 2(2): 115–118.

Raoof M and Davies TJ (2003) Simple determination of the axial stiffness for largediameter independent wire rope core or fibre core wire ropes. *The Journal of Strain Analysis for Engineering Design* 38(6): 577–586.

Raoof SM, Koutas LN and Bournas DA (2017) Textile-reinforced mortar (TRM) versus fibre-reinforced polymers (FRP) in flexural strengthening of RC beams. *Construction and Building Materials* 151: 279–291.

Rashedi SH, Rahai A and Tehrani P (2022) Seismic performance evaluation of RC bearing wall structures. *Computers and Concrete* 30(2): 113–126.

Rasheed HA, Abdalla J, Hawileh R, et al. (2017) Flexural behavior of reinforced concrete beams strengthened with externally bonded aluminum alloy plates. *Engineering Structures* 147: 473–485.

Rashid K, Li X, Deng J, et al. (2019) Experimental and analytical study on the flexural performance of CFRP strengthened RC beams at various pre-stressing levels. *Composite Structures* 227: 111323.

Razaqpur AG, Cameron R and Mostafa AAB (2020) Strengthening of RC beams with externally bonded and anchored thick CFRP laminate. *Composite Structures* 233: 111574.

Rezazadeh M, Costa I and Barros J (2014) Influence of prestress level on NSM CFRP laminates for the flexural strengthening of RC beams. *Composite Structures* 116(1): 489–500.

Saribiyik A, Abodan B and Balci MT (2021) Experimental study on shear strengthening of RC beams with basalt FRP strips using different wrapping methods. *Engineering Science and Technology, an International Journal* 24(1): 192–204.

Sen T and Reddy HNJ (2011) A numerical study of strengthening of RCC beam using natural bamboo fibre. *International Journal of Computer Theory and Engineering* 3(5): 707–713.

Shang XY, Yu JT, Li LZ, et al. (2019) Strengthening of RC structures by using engineered cementitious composites: a review. *Sustainability* 11(12): 3384.

Siddika A, Mamun MAA, Alyousef R, et al. (2019) Strengthening of reinforced concrete beams by using fiber-reinforced polymer composites: a review. *Journal of Building Engineering* 25: 100798.

Siddika A, Mamun MAA, Ferdous W, et al. (2020) Performances, challenges and opportunities in strengthening reinforced concrete structures by using FRPs – a state-of-the-art review. *Engineering Failure Analysis* 111: 104480.

Sim JI, Yang KH and Shim HJ (2009) Test on seismic strengthening of RC columns using wire rope and T-plate units. *Magazine of Concrete Research* 61(10): 823–836.

SNI 2052: 2014 (2014) *Steel Reinforcement of Concrete [in Indonesian]*. Jakarta, Indonesia: National Standardization Agency of Indonesia.

Sun X, Ma Y, Jiang F, et al. (2024) Bending resistance mechanism of prestressed ultra-high performance concrete-reinforced concrete beam based on a full-scale experiment. *Advances in Structural Engineering* 0(0).

Tang TT, Peng KD, Huang JQ, et al. (2024) Flexural performance of reinforced concrete beams strengthened with FRP-reinforced geopolymer matrix: numerical validation and parametric study. *Advances in Structural Engineering* 27(2): 269–287.

Tehrani BN, Mostofinejad D and Hosseini SM (2019) Experimental and analytical study on flexural strengthening of RC beams via prestressed EBROG CFRP plates. *Engineering Structures* 197: 109395.

Teng JG, Smith ST, Yao J, et al. (2003) Intermediate crack-induced debonding in RC beams and slabs. *Construction and Building Materials* 17(6–7): 447–462.

Tudjono S, Lie HA and Hidayat BA (2015) An experimental study to the influence of fiber reinforced polymer (FRP) confinement on beams subjected to bending and shear. *Procedia Engineering* 125: 1070–1075.

Tudjono S, Lie HA and Gan BS (2018) An integrated system for enhancing flexural members' capacity via combinations of the fiber reinforced plastic use, retrofitting, and surface treatment techniques. *International Journal of Technology* 9(1): 5–15.

van Mier JGM (1986) Multiaxial strain-softening of concrete. *Materials and Structures* 19(3): 179–190.

Wei Y and Wu YF (2014) Compression behavior of concrete columns confined by high strength steel wire. *Construction and Building Materials* 54: 443–453.

Woo SK, Nam JW, Kim JHJ, et al. (2008) Suggestion of ;exural capacity evaluation and prediction of prestressed CFRP strengthened design. *Engineering Structures* 30(12): 3751–3763.

Wu G, Wu ZS, Jiang JB, et al. (2010) Experimental study of RC beams strengthened with distributed prestressed high-strength steel wire rope. *Magazine of Concrete Research* 62(4): 253–265.

Wu G, Wu Z, Wei Y, et al. (2014) Flexural strengthening of RC beams using distributed prestressed high strength steel wire rope: theoretical analysis. *Structure and Infrastructure Engineering* 10(2): 160–174.

Xu Q, Chen X, Chen J-F, et al. (2019) Seismic strengthening of masonry walls using bamboo components. *Advances in Structural Engineering* 22(2): 2982–2997.

Xue WC, Tan Y and Zeng L (2010) Flexural response predictions of reinforced concrete beams strengthened with prestressed CFRP plates. *Composite Structures* 92(3): 612–622.

Yang KH and Ashour AF (2007) Tests of reinforced concrete short columns laterally strengthened with wire rope units and steel elements. *Magazine of Concrete Research* 59(8): 547–557.

Yang DS, Park SK and Neale KW (2009) Flexural behaviour of reinforced concrete beams strengthened with prestressed carbon composites. *Composite Structures* 88(4): 497–508.

Yang KH, Ashour AF and Lee ET (2009a) Axial behaviour of reinforced concrete short columns strengthened with wire rope and T-shaped steel plate units. *Magazine of Concrete Research* 61(2): 143–154.

Yang KH, Joo DB, Sim JI, et al. (2012) In-plane seismic performance of unreinforced masonry walls strengthened with unbonded prestressed wire rope units. *Engineering Structures* 45: 449–459.

Yang KH, Byun HY and Ashour AF (2009b) Shear strengthening of continuous reinforced concrete T-beams using wire rope units. *Engineering Structures* 31: 1154–1165.

Yang X, Gao W-Y, Dai J-G, et al. (2018) Flexural strengthening of RC beams with CFRP grid-reinforced ECC matrix. *Composite Structures* 189: 9–26.

Yin S, Xu S and Lv H (2014) Flexural behavior of reinforced concrete beams with TRC tension zone cover. *Journal of Materials in Civil Engineering* 26(2): 320–330.

You YC, Choi KS and Kim JH (2012) An experimental investigation on flexural behavior of RC beams strengthened with prestressed CFRP strips using a durable anchorage system. *Composites Part B: Engineering* 43(8): 3026–3036.

Zhang HY, Yan J, Kodur V, et al. (2019) Mechanical behavior of concrete beams shear strengthened with textile reinforced geopolymer mortar. *Engineering Structures* 196: 109348.

Zhang K, Shen X, Liu J, et al. (2022) Flexural strengthening of reinforced concrete T-beams using a composite of prestressed steel wire ropes embedded in polyurethane cement (PSWR-PUC): theoretical analysis. *Structures* 44: 1278–1287.

Zheng Y-Z, Wang W-W, Mosalam KM, et al. (2020) Experimental investigation and numerical analysis of RC beams shear strengthened with FRP/ECC composite layer. *Composite Structures* 246: 112436.

Zhou Y, Zhang J, Li W, et al. (2020) Reliability-based design analysis of FRP shear strengthened reinforced concrete beams considering different FRP configurations. *Composite Structures* 237: 111957.